Quantum Electronics **48** (2) 165–172 (2018)

LASER BEAMS https://doi.org/10.1070/QEL16411

Effects of phase singularity in the interference of two laser fields with a wide spectrum

O.M. Vokhnik, V.I. Odintsov

Abstract. **The interference of laser beams with a wide spectrum is studied theoretically and numerically. It is shown that in the cross section of such intersecting beams in a small vicinity of zero of the complex mutual coherence function, the change in the argument of the slow amplitude of this function corresponds to the phase singularity. An approximate analytical representation of the mutual coherence function in the vicinity of the singularity point is given. It is found that an average 'funnel' diameter of the modulus of the mutual coherence function that arises in the singularity region does not depend on the intensity of the light beams and remains constant when the longitudinal coordinate changes. The emergence of phase dislocations in the interference pattern is established.**

Keywords: *phase singularity, interference, correlation functions, laser fields with a wide spectrum.*

1. Introduction

Well-studied phase singularities in monochromatic light fields, also called optical vortices, arise at points where the field amplitude is zero and the phase is uncertain [1, 2].

Of no less interest are nonmonochromatic partially coherent fields, in which there are no regions where the amplitude vanishes, and phase singularities do not arise. At the same time, the singular behaviour reveals the correlation functions of such fields, which describe their coherent properties.

The singular behaviour of the phase of the spectral degree of coherence was reported in theoretical work [3], where two pinholes on an opaque screen illuminated by partially coherent light were the source of the field. In this paper, the concepts of singular optics were first extended to correlation functions. In a theoretical analysis of coherent properties of a partially coherent vortex-free field of another kind, i.e. the superposition of Hermite–Gaussian modes, Gbur and Visser [4] showed that in this field there exist pairs of points in which the spectral degree of coherence vanishes, and the phase of the spectral coherence function has a vortex structure in the vicinity of these points (thus, the term 'coherence vortex' was introduced). Subsequently, the spectral degree of coherence of various partially spatially coherent fortex-free and vortex light fields has been investigated by many authors (see, for example, [5–15]).

O.M. Vokhnik, V.I. Odintsov Faculty of Physics, M.V. Lomonosov Moscow State University, Vorob'evy Gory, 119991 Moscow, Russia; e-mail: vokhnik@rambler.ru

Received 17 April 2017; revision received 11 August 2017
Kvantovaya Elektronika **48** (2) 165–172 (2018)
Translated by I.A. Ulitkin

For a vortex-free noncoherent superposition of Laguerre–Gaussian modes of various orders, Bogatyryova et al. [5] found experimentally that the phase singularity of the spectral degree of coherence has the form of a circular edge dislocation. For a partially coherent vortex field, the singularity of the spatial coherence function in the form of a ring dislocation was first observed experimentally and investigated numerically in [6]. Yang et al. [7] obtained a dependence of the number of ring dislocations of a partially coherent vortex beam on the radial and azimuthal mode indices of the Laguerre–Gaussian mode. The helicoidal phase change of the complex coherence function was first experimentally demonstrated in [8] by the example of a spatially incoherent field, an optical vortex in which was introduced by a special zone plate.

A theoretical investigation of the spatial coherence function of a partially coherent field with singularities introduced into it by various configurations and its change with the beam propagation was carried out in [9, 10]. A generalised description of the correlation singularities using the four-variable transverse spectral density function proposed in [11] made it possible to interpret the experimental results obtained in [6] and [8] from a unified point of view. Paper [12] is devoted to the elucidation of the connection between phase singularities and coherence singularities, and paper [13] analyses the topology of the correlation singularities of partially coherent vortex beams. Stahl and Gbur [14] studied the evolution of the complete structure of the correlation singularity of such beams, including its description in the transverse plane and in the direction of propagation. The models of the investigated fields in [5–7, 11–14] were various modifications of the Laguerre–Gaussian beams. In a similar model used in [15], the measurement of the complex degree of coherence allowed the sign and magnitude of the topological charge of a partially coherent vortex beam to be simultaneously determined.

Another model of the optical beam, Gaussian–Schell (GSM) model, is widely used in the investigation of vector partially coherent beams with a spatially varying polarisation state (see, for example, [16–19]). The study of such beams is of interest both from a fundamental point of view and from the point of view of their use in various applications [16], and therefore the possibility of existence of correlation singularities in them and evolution of the properties of singular structures are of great importance. The propagation of a partially coherent vortex-free radially polarised beam in free space and in a turbulent atmosphere described by a non-Kolmogorov model was investigated in papers [17] and [18], respectively. The change in the statistical properties of such a beam with an optical vortex introduced into it was considered in [19]. Investigation of the correlation singularities of multi-Gaussian correlated Schell-model beams (so-called MGCSM beams)

made it possible to substantiate a method for determining the M-index of such beams with respect to the number of ring dislocations at a large distance from the source [20].

However, we note that for all the variety of partially coherent light beams whose correlation singular properties have been investigated, these are quasi-monochromatic fields in which the violation of spatial coherence is modelled in some specific way. The problems of existence and properties of the correlation singularities of the light with a large spectral width and random spatial structure, as well as manifestations of the phase singularity in the interference of two laser speckle fields with a wide spectrum (broadband fields), have scarcely been touched upon in the literature.

In this paper, we study theoretically the phase singularities of the correlation function of mutual coherence in the interference of two speckle fields with a random spatial structure and a wide frequency spectrum ($\Delta\omega \sim 1000$ cm^{-1}). With such a spectral width, the light field is coherent only in a $1/\Delta\omega \sim 10^{-3}$-cm-thick narrow layer (called a coherence layer and perpendicular to the direction of propagation). The spatial width of the interference region, even at a small angle between the beams, is much smaller than their diameters, which determines a small efficiency of coherent interaction of intersecting beams. To expand the region of coherent interaction of interfering beams, the method of introducing dispersion was used [21] (see below).

We propose an optical scheme for the interference of broadband beams of various spatial configurations. To estimate the degree of mutual coherence of interfering beams, which determines the efficiency of their coherent interaction in four-wave mixing schemes and in loop phase-conjugation schemes, we use the function of mutual coherence of two beams at one point of space, introduced in [22],

$$\Gamma(\boldsymbol{r}) = \overline{E_1(\boldsymbol{r},t)E_2^*(\boldsymbol{r},t)}, \qquad (1)$$

where the bar denotes averaging over time. It determines the interference contribution to the light intensity in the region of superposition of two fields with a wide spectrum

$$I(\boldsymbol{r}) = I_1(\boldsymbol{r}) + I_2(\boldsymbol{r}) + 2\mathrm{Re}\Gamma(\boldsymbol{r}), \qquad (2)$$

where $I_{1,2}$ is the intensity of each of the fields.

Based on the numerical simulation, we study the characteristics of the interference pattern. It is found that in the transverse plane z = const, including the initial plane, there exist points at which the modulus of the complex mutual coherence function vanishes, and the phase of its slow amplitude exhibits a singular behaviour, while the interfering beams are vortex-free. It is shown that the phase singularities of the mutual coherence function lead to the appearance of dislocations in a stationary interference pattern.

It is also shown that the phase singularities also take place for the slow amplitude of the generalised mutual coherence function (introduced in the present paper), which characterises the excitation of oscillations by light fields in a nonlinear medium that lead to stimulated scattering of light.

2. Analytical consideration

The complex function $f(x,y) = f'(x,y) + \mathrm{i}f''(x,y)$ vanishes at the point of intersection (x_0,y_0) of the 'zero lines' of the real and imaginary parts: $f'(x,y) = 0$ and $f''(x,y) = 0$. Upon passage around the zero point in the positive direction (counterclockwise), $\arg(f)$ increases by 2π. If $f'(x,y)$ and $f''(x,y)$ are uniform random functions with zero mean values, then the 'zero lines' in the xy plane form a grid with zero points at their intersections [23].

For an effective interaction of broadband light beams in a medium, a temporal variation of their envelopes in the entire region of beam superposition is needed. Light beams with mutually correlated coherence layers can be obtained by dividing one and the same source beam using a semitransparent mirror.

To increase the interaction region of the beams crossing at a small angle, their coherence layers are made parallel by tilting with respect to the axial directions; in this case, the width of the interaction region is limited only by the beam diameters. The necessary slope of the coherence layers is achieved by introducing dispersion [21]: the beams propagate through a dispersing element, for example a prism. In the prism, the slope of the coherence layers is due to the difference of the phase-front velocities from the group velocity with which the coherence layer moves. As a dispersing element use can be made of a diffraction grating with a triangular profile of grooves, operating in the same diffraction order (see below).

We assume that in the initial plane $z = 0$ both interfering beams are spatially coherent and correlated with time. The interference of such light beams can be provided by a scheme based on a Mach–Zehnder interferometer with diffraction gratings (see Fig. 1). A broadband plane light beam (LB) falls on a semitransparent beam-splitting mirror M1. The coherence layer of thickness $l_c = 1/\Delta\omega$ is oriented perpendicular to the direction of the incident wave. The separated light beams LB1 and LB2 pass through thin amplitude–phase transparencies T1 and T2, introducing random phase and amplitude changes into the beams. They are installed in front of the same diffraction gratings DG1 and DG2. Diffraction gratings with the orientation of the grooves perpendicular to the plane of the pattern operate in opposite diffraction orders: $m_2 = -m_1$. The directions of the incident and diffracted light beams are shown by arrows. The dispersed beams DB1 and DB2 coming out of the two arms of the interferometer are superimposed by means of a folding mirror M3 and a semitransparent mirror M4. An inclined glass plate Pl serves to equalise the optical lengths of the arms of the interferometer, which makes it possible to combine parallel correlated coherence layers in interfering dispersed beams DB1 and DB2.

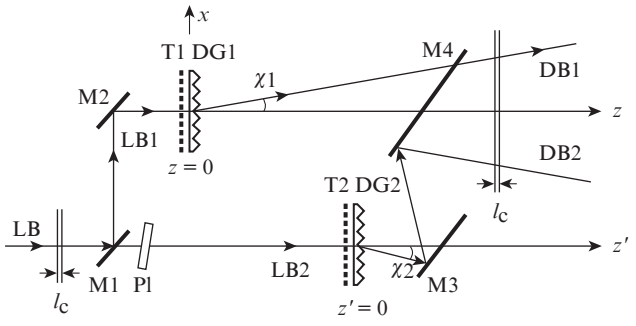

Figure 1. Interference scheme for dispersed light beams: (LB) incident light beam; (LB1, LB2) beams in the arms of the interferometer; (DB1, DB2) dispersed beams; (M1, M4) semitransparent mirrors; (M2, M3) folding mirrors; (T1, T2) amplitude–phase transparencies; (DG1, DG2) diffraction gratings; (l_c) coherence layers of the incident and two dispersed beams; (Pl) plane-parallel glass plate.

We assume that the imaginary images in the system of mirrors M1 and M2, the z' axis, the $z' = 0$ plane, as well as in the planes in which the transparency T2 and the diffraction grating DG2 are located, are aligned respectively with the z axis, the $z = 0$ plane and the planes of the transparency T1 and the diffraction grating DG1 in the upper arm of the interferometer.

The diffraction grating DG1 (DG2), operating in one diffraction order m_j ($j = 1, 2$ is the number of the grating) and set perpendicular to the z axis, converts a monochromatic plane wave incident on it with the wave vector $\boldsymbol{k}(\omega,\boldsymbol{\alpha}_0)$ [$\alpha_0 = \boldsymbol{k}(\omega,\boldsymbol{\alpha}_0)_\perp$ is the component of the wave vector $\boldsymbol{k}(\omega,\boldsymbol{\alpha}_0)$ perpendicular to the z axis] to a plane wave with the wave vector $\boldsymbol{k}(\omega,\boldsymbol{\alpha})$, where $\boldsymbol{\alpha} = \boldsymbol{\alpha}_0 + \boldsymbol{a}_j$, the vector $\boldsymbol{a}_j$ is perpendicular to the z axis and to the direction of the grating grooves, $|\boldsymbol{a}_j| = |m_j|(2\pi/d_j)$, and d_j is the grating period. The axial direction of the broadband dispersed light beam after the grating is given by the vector $\boldsymbol{k}(\bar{\omega},\boldsymbol{a}_j)$, where $\bar{\omega}$ is the mean frequency of the radiation. It forms with the z axis the angle χ_j, equal to the deviation angle of the corresponding grating for the frequency $\bar{\omega}$. If the x-axis orientation is perpendicular to the primes, we obtain $\sin\chi_j = a_j/|\boldsymbol{k}(\bar{\omega})|$, where $a_j = m_j(2\pi/d_j)$ is the projection of the vector $\boldsymbol{a}_j$ onto the x axis.

After the passage of light beams through the diffraction grating, the orientation of the coherence layers does not change: both in the diffracted and in the incident beam they are perpendicular to the z axis. Thus, the axial direction of the dispersed light beam is deviated from the normal to the coherence layers by the angle χ_j. In the scheme described above, the coherence layers of the interfering light beams DB1 and DB2 are parallel to one another, and the angle of intersection of the beams $\psi_j = |\chi_1 - \chi_2|$ for $d_1 = d_2 = d$ and $|m_j| = 1$ is $2\bar{\lambda}/d$. Note that along with the described optical scheme, use can be made of a scheme with reflective diffraction gratings installed as end mirrors of the Michelson interferometer.

The fields of the interfering light beams can be represented as a superposition of monochromatic components:

$$E_j(\boldsymbol{r},t) = \int_0^\infty \varepsilon_j(\omega)\exp(\mathrm{i}\omega t)E_{j\omega}(\boldsymbol{r})\,\mathrm{d}\omega, \tag{3}$$

where

$$E_{j\omega}(\boldsymbol{r}) = \int \varepsilon_j(\boldsymbol{\alpha})\exp[-\mathrm{i}\boldsymbol{k}(\omega,\boldsymbol{\alpha})\boldsymbol{r}]\,\mathrm{d}\boldsymbol{\alpha}. \tag{4}$$

When the correlated coherence layers of both beams are combined, in expression (3) we can put

$$\varepsilon_1(\omega) = \varepsilon_2(\omega) = \varepsilon(\omega). \tag{5}$$

Representing the time variation of the field incident on the beam-splitting mirror M1 as a stationary random process, and the transverse spatial field distribution after each of the transparencies T1, T2 as a homogeneous Gaussian random process, we introduce the normalised spectral densities $\eta(\omega)$ and $\eta(\boldsymbol{\alpha})$ by the relations [24]

$$\overline{\varepsilon(\omega)\varepsilon^*(\omega')} = \eta(\omega)\delta(\omega - \omega'), \tag{6}$$

$$\frac{cn}{8\pi}\langle\varepsilon_j(\boldsymbol{\alpha})\varepsilon_j^*(\boldsymbol{\alpha}')\rangle = \langle I_j\rangle\eta_j(\boldsymbol{\alpha})\delta(\boldsymbol{\alpha} - \boldsymbol{\alpha}'), \tag{7}$$

where the bar denotes averaging over temporal field realisations, and the angle brackets mean averaging over the realisations of the transverse spatial distribution of the field that arises when different statistically uniform transparencies T1 and T2 are installed; and $\langle I_j\rangle$ is the cross-section averaged intensity of the light beam.

Due to the deviation of the dispersed beam, the relation $\eta_j(\boldsymbol{\alpha}) = \eta_j^0(\boldsymbol{\alpha} - \boldsymbol{a}_j)$ is valid, where $\eta_j^0(\boldsymbol{\alpha})$ is the spectral power density of the light beam incident on the corresponding diffraction grating. In what follows, we assume $\eta_1^{(0)}(\boldsymbol{\alpha}) = \eta_2^{(0)}(\boldsymbol{\alpha}) = \eta^{(0)}(\boldsymbol{\alpha})$.

We introduce slowly varying amplitudes $A_{j\omega}(\boldsymbol{r})$ of the fields, assuming for $\boldsymbol{a}_1 = \boldsymbol{a}$ and $\boldsymbol{a}_2 = -\boldsymbol{a}$

$$\begin{aligned} E_{1\omega}(\boldsymbol{r}) &= A_{1\omega}(\boldsymbol{r})\exp(-\mathrm{i}\boldsymbol{k}(\omega,\boldsymbol{a})\boldsymbol{r}),\\ E_{2\omega}(\boldsymbol{r}) &= A_{2\omega}(\boldsymbol{r})\exp(-\mathrm{i}\boldsymbol{k}(\omega,-\boldsymbol{a})\boldsymbol{r}). \end{aligned} \tag{8}$$

The mutual coherence function $\Gamma(\boldsymbol{r})$ can be represented in the form

$$\Gamma(\boldsymbol{r}) = \int_0^\infty \Gamma_\omega(\boldsymbol{r})\eta(\omega)\,\mathrm{d}\omega, \tag{9}$$

where

$$\Gamma_\omega(\boldsymbol{r}) = E_{1\omega}(\boldsymbol{r})E_{2\omega}^*(\boldsymbol{r}). \tag{10}$$

From relations (8) and (10), with allowance for $\boldsymbol{a} \parallel \mathrm{O}x$, we have

$$\Gamma_\omega(\boldsymbol{r}) = B_\omega(\boldsymbol{r})\exp(-\mathrm{i}2ax), \tag{11}$$

where $B_\omega(\boldsymbol{r}) = A_{1\omega}(\boldsymbol{r})A_{2\omega}^*(\boldsymbol{r})$.

From (9) and (11) we obtain

$$\Gamma(\boldsymbol{r}) = B(\boldsymbol{r})\exp(-\mathrm{i}2ax), \tag{12}$$

where

$$B(\boldsymbol{r}) = \int_0^\infty B_\omega(\boldsymbol{r})\eta(\omega)\,\mathrm{d}\omega \tag{13}$$

is the slowly varying amplitude of the function $\Gamma(\boldsymbol{r})$; $B(\boldsymbol{r}) = B'(\boldsymbol{r}) + \mathrm{i}B''(\boldsymbol{r})$; and $|\Gamma(\boldsymbol{r})| = |B(\boldsymbol{r})|$.

Exception for the regions of the phase singularity – small vicinities of zero points (see below) – the characteristic scale of the variation of $B(\boldsymbol{r})$ with respect to x and y is estimated as $r_{\mathrm{cor}} = \bar{\lambda}/2\theta$, where r_{cor} is the correlation radius of the speckle field (the transverse size of the speckle spots); $\bar{\lambda}$ is the average wavelength; and 2θ is the angular divergence of the radiation. If the angle between the interfering beams is $\psi \gg 2\theta$, then r_{cor} is much larger than the distance between the interference bands $\Lambda = \bar{\lambda}/\psi$.

3. Calculation of the mutual coherence function

Two approaches were used in this paper: numerical simulation, which allows one to obtain two-dimensional distributions of the amplitude and phase of the mutual coherence function in the cross section of intersecting beams, $z = \mathrm{const}$;

and the linear approximation method based on approximate analytical expressions.

3.1. Numerical simulation

In the numerical simulation of the function $\Gamma(\boldsymbol{r})$ and the slow amplitude $B(\boldsymbol{r})$, the calculation began with the computation of the fields $E_{j\omega}(\boldsymbol{r})$ in accordance with (4). On a discrete set of values of α_x,α_y, we used a random number generator to set the real and imaginary parts of the complex amplitudes $\varepsilon_j(\boldsymbol{\alpha})$, distributed according to the Gaussian law with the variance $4\pi/(cn)\langle I\rangle\eta(\alpha_x,\alpha_y)\,\delta\alpha_x\delta\alpha_y$ [$\langle I\rangle$ is the average intensity of the initial broadband uniform plane wave, and $\delta\alpha_x$ and $\delta\alpha_y$ are the intervals between the discrete values of α_x and α_y]. The two independent sets of complex amplitudes $\varepsilon_{1,2}(\boldsymbol{\alpha})$ obtained in this way were used in (4) to calculate the fields $E_{j\omega}(\boldsymbol{r})$ and then in accordance with formulas (9)–(13) to determine $\Gamma(\boldsymbol{r})$ and $B(\boldsymbol{r})$.

In this section, as well as in Section 4, calculations were performed at a centre wavelength $\bar{\lambda} = 10^{-4}$ cm, spectral width $\Delta\omega = 1000$ cm^{-1} (the ratio $\Delta\omega/\omega$ was 0.1) and Gaussian frequency spectrum. Note that this relation holds for a promising carbon monoxide laser.

The angular divergence $2\theta_0$ of the initial beam was assumed to be 4×10^{-3} rad, and the deflection angles of the diffraction gratings were $|\chi_j| = 2\times10^{-2}$ rad. The angle between the interfering beams, $\psi = 4\times10^{-2}$ rad, was an order of magnitude greater than their angular width.

3.2. Linear approximation

In the fixed plane z = const, in a small vicinity of zero of the function $B(\boldsymbol{r})$ with coordinates x_0, y_0, the approximate representation

$$B(x,y,z) \approx P_0(x-x_0) + Q_0(y-y_0) \tag{14}$$

is valid, where

$$P_0 = P_0' + \mathrm{i}P_0'' = \left.\frac{\partial B}{\partial x}\right|_{x_0,y_0},\ Q_0 = Q_0' + \mathrm{i}Q_0'' = \left.\frac{\partial B}{\partial y}\right|_{x_0,y_0} \tag{15}$$

are the complex derivatives $B(x,y,z)$ with respect to x and y at the zero point (x_0,y_0); and $|x-x_0|$, $|y-y_0| \ll r_{\mathrm{cor}}$. Passing to the polar coordinate system ρ and ϑ, we set $x-x_0 = \rho\cos\vartheta$, $y-y_0 = \rho\sin\vartheta$, and, denoting $\hat{\Phi}_B = \arg B$, we obtain from (14) and (15)

$$\tan\hat{\Phi}_B = \frac{P_0''\cos\vartheta + Q_0''\sin\vartheta}{P_0'\cos\vartheta + Q_0'\sin\vartheta}. \tag{16}$$

If the point with the coordinates x,y moves along a straight line passing through the zero point, then in accordance with (14) and (16) the phase $\hat{\Phi}_B(x,y) = \hat{\Phi}_B(\vartheta)$ remains unchanged and only changes jumpwise by $\pm\pi$ after passing through the zero point. Therefore, in a small vicinity of the zero point

$$\hat{\Phi}_B(\vartheta\pm\pi) = \hat{\Phi}_B(\vartheta)\pm\pi. \tag{17}$$

With a symmetrical arrangement of the zero lines relative to the coordinate axes x and y (as shown below in Fig. 4), expression (16) yields the relation

$$\tan\hat{\Phi}_B = S\frac{\tan(\gamma/2)\cos\vartheta + \sin\vartheta}{\tan(\gamma/2)\cos\vartheta - \sin\vartheta}, \tag{18}$$

where $S = P_0''/P_0'$; and $\gamma \leqslant \pi/2$ is the angle between the zero lines. Setting $\hat{\Phi}_B = 3\pi/4$ for $\vartheta = 0$, we obtain $S = -1$ from (18), which will be used below in the calculations.

4. Mutual coherence function in the vicinity of an isolated point of singularity

4.1. Distribution of the slow amplitude of the mutual coherence function $B(x,y)$ in the z = const plane

Figures 2a and 2b show numerically simulated two-dimensional distributions of the modulus and phase of the slowly varying amplitude $B(x,y)$ in the vicinity of the zero point at

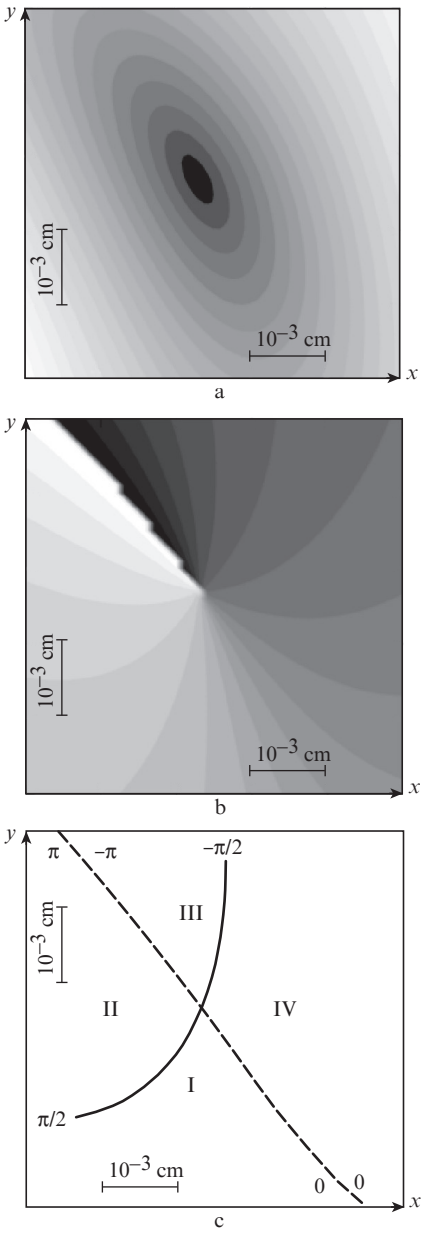

Figure 2. Distributions in the vicinity of (a) the zero point $|B(x,y)|$ and (b) phase $\Phi_B = \arg B(x,y)$ and (c) zero lines $B'(x,y) = 0$ (solid curve) and $B''(x,y) = 0$ (dashed curve).

$z = 1$ cm. The lighter areas correspond to large values of $|B|$ and $\Phi_B = \arg B$. Figure 2c illustrates the zero lines of the real and imaginary parts of $B(x, y)$, intersecting at the zero point (x_0, y_0), and the quadrants in the complex plane and the boundary values of the phase Φ_B. The two-dimensional phase distribution in Fig. 2b is in good agreement with the zero-line trajectory in Fig. 2c and clearly demonstrates an increase in $\hat{\Phi}_B$ by 2π upon passage around the zero point.

Figure 3a shows the dependences of $|B|$ and Φ_B on x, obtained by numerical simulation for $y = y_0$ and $z = 25$ cm. For comparison, we present also the dependence of $|B|$ on x calculated in the linear approximation by formula (14) using the numerically obtained values of P_0 and Q_0. The lower part of the curve $|B(x_0, y_0)|$ is given on the right on an enlarged scale. It is clearly seen that for $x = x_0$ the phase $\Phi_B(x, y_0)$ changes abruptly by π, which agrees with (17).

The dependence of the phase $\Phi_B(x, y)$ on x for various values of $y = \text{const}$ is given in Fig. 3b. In the case of $y = y_0$ (solid line), when passing through the zero point, there is a phase jump of Φ_B by π. The dependence of $\Phi_B(x, y)$ on x for $y \neq y_0$ has a more complicated form, when the point (x, y) moves along a straight line that does not pass through the zero point. In this case, it intersects lines passing through the zero point at different angles ϑ, the phase $\hat{\Phi}_B(\vartheta)$ on which is given by expression (16). The number of intersecting straight lines per unit displacement of the point (x, y) along x increases with an approach of x to x_0; in this case, the phase $\Phi_B(x, y)$ changes faster. The curves in Fig. 3b (dashed curve for $y = y_0 + 0.5\bar{\lambda}$ and dotted curve for $y = y_0 + 2\bar{\lambda}$) represent a specific form of this dependence in a small vicinity of the zero point; they also show that the smaller the deviation of y from y_0, the closer the dependence of $\Phi_B(x, y)$ to the abrupt one. For $x = x_0$, the curves with different values of y intersect at one point, since $\vartheta = \pi/2$ and the phase Φ_B, which is equal to $\arctan(Q_0'' / Q_0')$ in the linear approximation in accordance with formula (16), does not depend on y.

In Fig. 3c, the change in the phase Φ_B upon bypassing the zero point with a small radius $R < 3 \times 10^{-3}$ cm does not depend on R, which agrees with (16). In this case, relation (17) holds with good accuracy. Spatial phase fluctuations strictly azimuthal at small radii of bypassing seem to be of a general nature with the mutual coherence fluctuations investigated in [22]. A comparison of the dependences of $|B|$ on x calculated numerically and in the linear approximation, as well as the results presented in Fig. 3, show that the linear approximation describes well the behaviour of the slow amplitude $B(x, y)$ in the vicinity of the zero point with a radius less than 3×10^{-3} cm.

4.2. Phase distribution of the mutual coherence function $\Gamma(x, y)$ in the $z = \text{const}$ plane

According to (12), the phase of the function $\Gamma(x, y)$ can be written as

$$\Phi_\Gamma(x, y) = \Phi_B(x, y) - 2ax. \tag{19}$$

Figure 4 shows the phase lines $\Phi_\Gamma(x, y) = \text{const}$, obtained from (19) and (18) at $S = -1$ and $\gamma = 60°$. If we assume $B =$

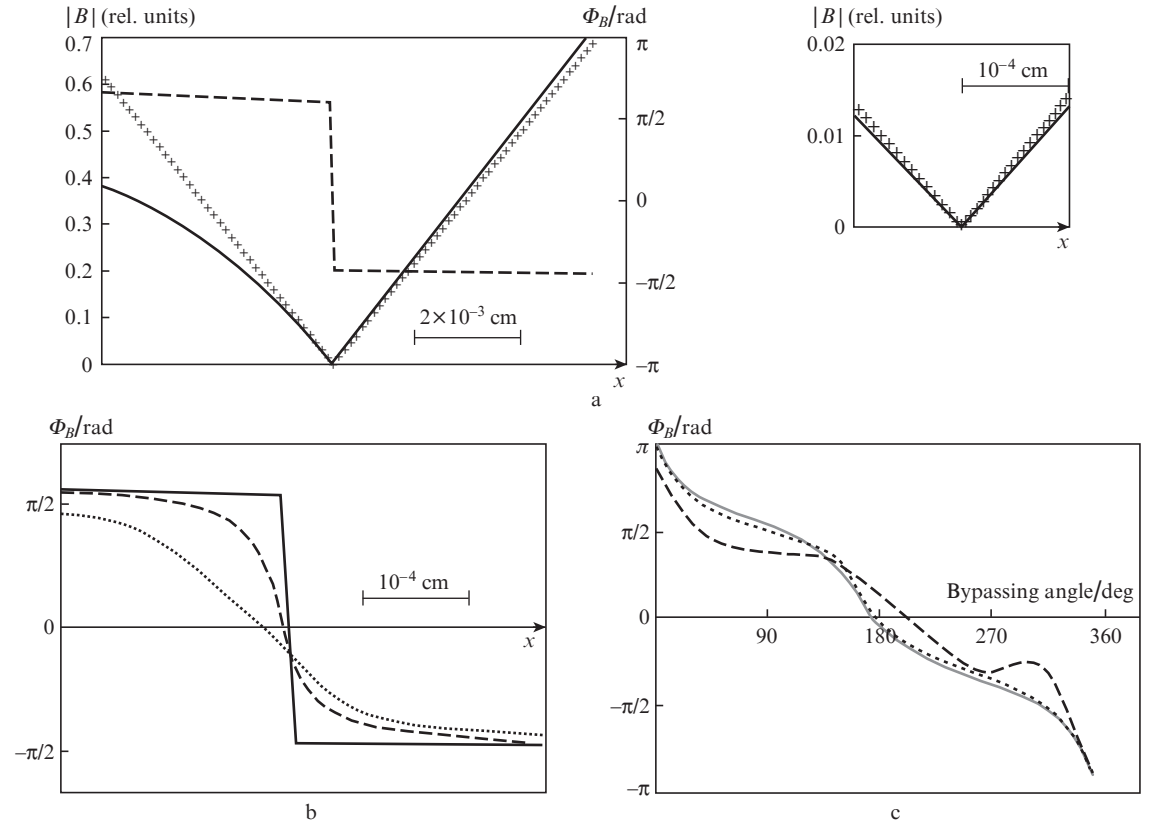

Figure 3. (a) Numerically simulated dependences of $|B(x, y_0)|$ (solid curve) and $\Phi_B(x, y_0)$ (dashed curve) on x, as well as the calculation results in the linear approximation (shown by crosses); (b) dependences of $\Phi_B(x, y_0)$ on x at $y = y_0$ (solid curve), $y = y_0 + 5 \times 10^{-5}$ cm (dashed curve) and $y = y_0 + 2 \times 10^{-4}$ cm (dotted curve); (c) change in the phase of the function Φ_B upon bypassing the zero point with a radius 1.5×10^{-3} cm (solid curve), 2.5×10^{-3} cm (dashed curve) and 7.5×10^{-3} cm (dotted curve).

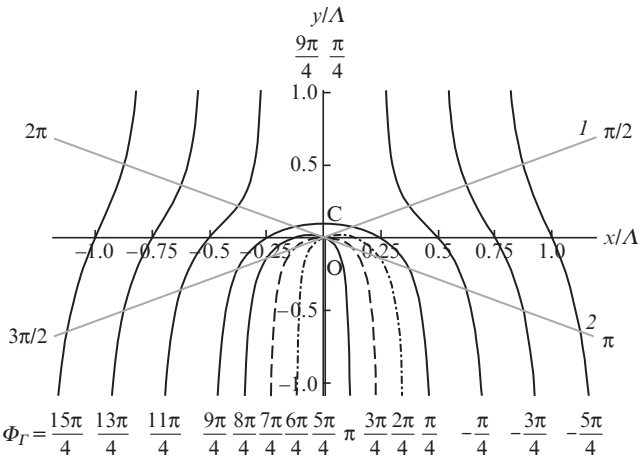

Figure 4. Phase lines $\Phi_\Gamma(x,y)$ = const in the vicinity of an isolated singularity point [the angle γ between the zero lines (*1*) and (*2*) is 60°].

const in (12), then the set of phase lines with different values of the Φ_Γ has the form of rectilinear bands repeating with a period $\Lambda = \pi/a$. The presence of the dependence of B on x, y disrupts the regular pattern of the bands.

The phase lines with $\Phi_B(x,y) = \pi/4$ and $9\pi/4$, emerging from the instability point C perpendicular to the y axis, deflect into the region of negative values of y and form a 'fork' inside which the phase lines pass through the zero point O. Analogous 'forks' in the vicinity of points of phase singularity arise also with the interference of monochromatic light beams [25].

The coordinate y_C of point C is determined from the equation

$$\frac{\mathrm{d}\Phi_B(x,y_C)}{\mathrm{d}x} = 2a. \tag{20}$$

From expressions (18) at $S = -1$ and (20) one can obtain

$$y_C \approx 1/(2a)\tan(\gamma/2). \tag{21}$$

The course of the phase lines near points O and C is shown in Fig. 5a. It follows from (19) and (20) that at point C, $\mathrm{d}\Phi_\Gamma/\mathrm{d}x = 0$. As can be seen from the figure, in the vicinity of point C the phase $\Phi_\Gamma(x,y)$ depends weakly on the coordinates x, y and remains close to $\pi/4$. The position of the intersection points of the phase lines with the y axis for different angles γ between the zero lines, presented in Fig. 5b, agrees well with formula (21).

Figure 6a shows the numerically simulated two-dimensional distribution of the phase $\Phi_\Gamma = \arg\Gamma(x,y)$ in the vicinity of the zero point. As in Fig. 2b, the lighter areas correspond to larger values of the phase. The phase singularity of the slow amplitude $B(x,y)$ manifests itself in the presence of a characteristic 'fork' near the zero point in the spatial distribution of the phase $\Phi_\Gamma(x,y)$, which also appears in the intensity of the interference pattern shown in Fig. 6b.

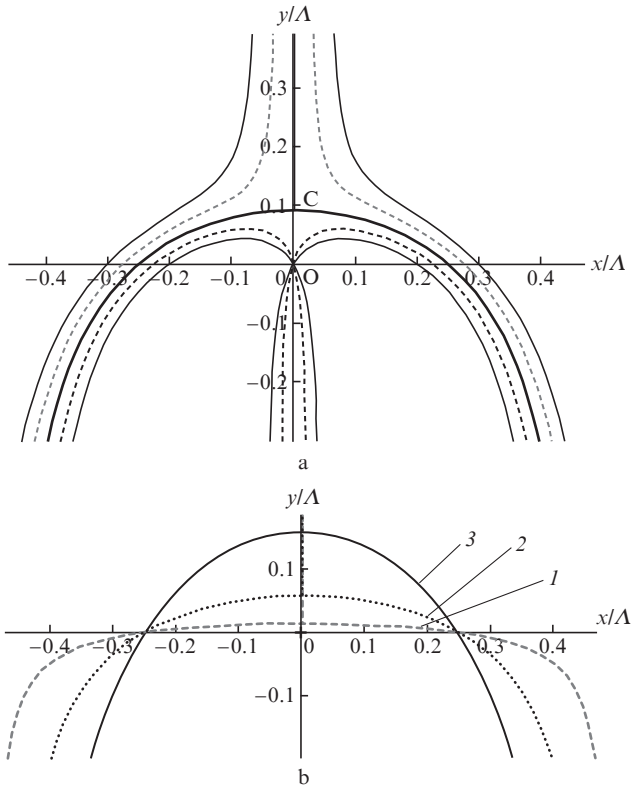

Figure 5. Phase lines $\Phi_\Gamma(x,y)$ = const near the instability point C: (a) $\Phi_\Gamma = \pi/4$ and $9\pi/4$ (thick solid curve), $\pi/4 \pm \pi/20$ and $9\pi/4 \pm \pi/20$ (dashed curves) and $\pi/4 \pm \pi/10$ and $9\pi/4 \pm \pi/10$ (thin solid curves) at $\gamma = 60°$, as well as (b) $\Phi_\Gamma = \pi/4$ and $9\pi/4$ at $\gamma =$ (*1*) 10°, (*2*) 40° and (*3*) 90°.

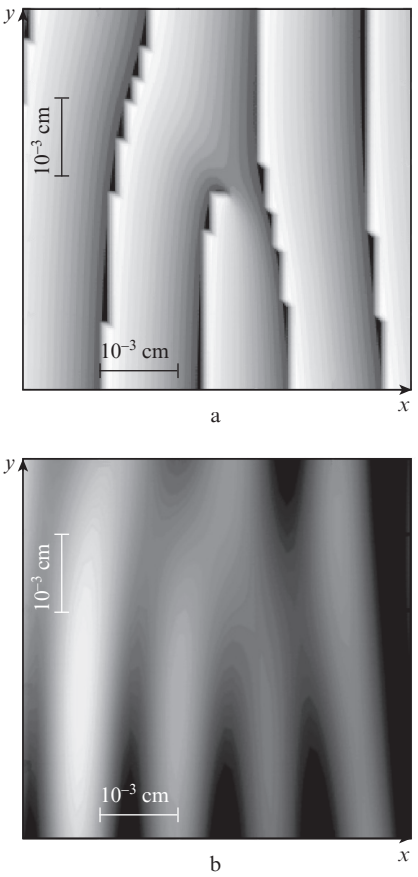

Figure 6. (a) Distribution in the vicinity of the zero point of the phase of the mutual coherence function $\Phi_\Gamma = \arg\Gamma(x,y)$ and (b) the intensity of the interference pattern.

5. Determination of $|B(x,y)|$ in the region of singularity as a function of z, using statistical characteristics

The spatial coherence of each broadband light beam and the mutual coherence of two interfering light beams decrease with distance from the initial plane $z = 0$, in which such radiation is assumed to be spatially coherent.

We assume $P(x,y,z) = \partial B(x,y,z)/\partial x$ and use an analytical calculation for the Gaussian shape of the spectrum $\eta^{(0)}(\alpha)$ to find the root-mean-square quantities

$$\tilde{B}(z) = \sqrt{\left\langle \left| B(x,y,z) \right|^2 \right\rangle} \text{ и } \tilde{P}(z) = \sqrt{\left\langle \left| P(x,y,z) \right|^2 \right\rangle}.$$

They do not depend on the frequency spectrum $\eta_0(\omega)$, and their values in the initial plane $z = 0$ are determined by expressions

$$\begin{aligned} \tilde{B}(0) &= 8\pi/(cn)\sqrt{\langle I_1\rangle\langle I_2\rangle}, \\ \tilde{P}(0) &= 8\pi/(cn)\sqrt{\langle I_1\rangle\langle I_2\rangle}(k(\bar{\omega})\theta/\sqrt{\ln 2}). \end{aligned} \tag{22}$$

The calculation showed that the quantities $\tilde{B}(z)$ and $\tilde{P}(z)$ change similarly with z, such that

$$\tilde{B}(z)/\tilde{B}(0) = \tilde{P}(z)/\tilde{P}(0) = H(z). \tag{23}$$

The dependence $H(z)$ is shown in Fig. 7. The obtained dependence $\tilde{B}(z)$ agrees with the results of [22], which describes the visual mechanism of a decrease in mutual coherence upon propagation of light beams.

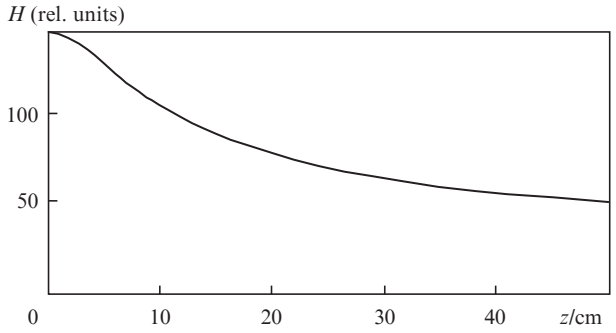

Figure 7. Dependence of the mutual coherence of the beams on the longitudinal coordinate z for $\tilde{B}(z)/\tilde{B}(0) = \tilde{P}(z)/\tilde{P}(0) = H(z)$.

Under the conditions of fulfilment of the linear approximation, from (14) with $P_0 = Q_0$ it follows that in the fixed plane $z = \hat{z} = \text{const}$ the transverse distribution $|B(x,y,\hat{z})|$ has the form of an inverted cone of circular cross section ('funnel'). The 'funnel', in which $P_0 = Q_0 = \tilde{P}(z)$ and the height is equal to $\tilde{B}(z)$, is called average statistical. The opening angle of such a funnel $\tilde{\beta}(z) = 1/\tilde{P}(z)$ increases with increasing z, and the diameter of the hole remains constant, $\tilde{D} = 2\tilde{B}(z)/\tilde{P}(z) = 2\tilde{B}(0)/\tilde{P}(0)$. Taking (22) into account, we have

$$\tilde{D} = 2\sqrt{\ln 2}/(k(\bar{\omega})\theta). \tag{24}$$

With an average wavelength of $\bar{\lambda} = 10^{-4}$ cm and an angular divergence of $2\theta = 4 \times 10^{-3}$ used in the calculations, we obtain from (24) $\tilde{D} = 1.32 \times 10^{-2}$ cm. This value is $\sqrt{2}$ times smaller than the analogous calculation of the 'funnel' diameter of intensity in the singularity region of a single monochromatic light beam with a wavelength equal to $\bar{\lambda}$.

6. Generalized mutual coherence function

The above-considered mutual coherence function $\Gamma(\boldsymbol{r})$ describes the interaction of two broadband light fields, which leads to the formation of a stationary interference pattern. The generalised mutual coherence function

$$\Gamma(\Omega,\boldsymbol{r}) = \overline{E_1(\boldsymbol{r},t)E_2^*(\boldsymbol{r},t)\exp(-\mathrm{i}\Omega t)} \tag{25}$$

is introduced to characterise the interaction of broadband fields (laser field E_1 and Stokes field E_2 frequency shifted in Ω), at which the interference pattern created by them at each point $\boldsymbol{r}$ varies harmoniously with time at the frequency Ω, and the interference fringes move in the cross section of the light beams. This causes the excitation of oscillations at the frequency Ω in a nonlinear medium and stimulated light scattering.

The generality of the mathematical description of $\Gamma(\Omega,\boldsymbol{r})$ and the mutual coherence function $\Gamma(\boldsymbol{r})$ studied above [see (9) and (10)] allows us to conclude that the slow amplitudes $\Gamma(\Omega,\boldsymbol{r})$ have singularities in the form of phase singularities which should lead to phase singularities of oscillations excited in a nonlinear medium, as well as to phase singularities in the emission of the Stokes component of stimulated light scattering.

7. Conclusions

We have studied theoretically the phase singularity of a slow amplitude of the mutual coherence function of two broadband laser fields, which leads to the appearance of dislocations in the interference pattern arising in the region of their superposition. A scheme has been proposed for experimental realisation of the interference of dispersed broadband laser beams based on a Mach–Zehnder interferometer with diffraction gratings.

The two-dimensional distributions of the modulus and the phase of the slow amplitude of the complex mutual coherence function in the cross section of intersecting light beams have been obtained by numerical simulation. An analytical description of the slow amplitude in the region of the phase singularity has been presented on the basis of the linear approximation.

The statistical characteristics of the mutual coherence function have been studied as a function of the longitudinal coordinate. The average diameter of the 'funnel' of the modulus of the mutual coherence function that arises in the singularity region has been calculated. It has been found that it does not depend on the intensity of the light beams and remains constant when the longitudinal coordinate changes.

The manifestation of phase dislocations in the interference pattern has been investigated. It has been shown that the phase singularities also occur for the introduced generalised mutual coherence function, which characterises the excitation of oscillations in the nonlinear medium resulting in stimulated light scattering. The results obtained can be used to study the effects of phase singularity in four-wave mixing

schemes with intersecting light beams, as well as in implementation of phase conjugation of broadband laser radiation.

References

1. Soskin M.S., Vasnetsov M.V. *Prog. Opt.*, **42**, 219 (2001).
2. Dennis M.R., O'Holleran K., Padgett M.J. *Prog. Opt.*, **53**, 293 (2009).
3. Schouten H.F., Gbur G., Visser T.D., Wolf E. *Opt. Lett.*, **28**, 968 (2003).
4. Gbur G., Visser T.D. *Opt. Commun.*, **222**, 117 (2003).
5. Bogatyryova G.V., Fel'de C.V., Polyanskii P.V., Ponomarenko S.A., Soskin M.S., Wolf E. *Opt. Lett.*, **28**, 878 (2003).
6. Palacios D.M., Maleev I.D., Marathay A.S., Swartzlander G.A. Jr. *Phys. Rev. Lett.*, **92**, 143905 (2004).
7. Yang Y., Chen M., Mazilu M., Mourka A., Liu Yi-D., Dholakia K. *New J. Phys.*, **15**, 113053-1 (2013).
8. Wang W., Duan Z., Hanson S.G., Miyamoto Y., Takeda M. *Phys. Rev. Lett.*, **96**, 073902 (2006).
9. Maleev I.D., Palacios D.M., Marathay A.S., Swartzlander G.A. Jr. *J. Opt. Soc. Am. B*, **21**, 1895 (2004).
10. Maleev I.D., Swartzlander G.A. Jr. *J. Opt. Soc. Am. B*, **25**, 915 (2008).
11. Gbur G., Swartzlander G.A. Jr. *J. Opt. Soc. Am. B*, **25**, 1422 (2008).
12. Van Dijk T., Visser T.D. *J. Opt. Soc. Am. A*, **26**, 741 (2009).
13. Van Dijk T., Schouten H.F., Visser T.D. *Phys. Rev. A*, **79**, 033805 (2009).
14. Stahl C.S.D., Gbur G. *Opt. Lett.*, **39**, 5985 (2014).
15. Chen J., Liu X., Yu J., Cai Y. *Appl. Phys. B*, **122**, 201 (2016).
16. Zhan Q. *Adv. Opt. Photon.*, **1**, 1 (2009).
17. Zhang Y., Cui Y., Wang F., Cai Y. *Opt. Express*, **23**, 11483 (2015).
18. Zhang Y., Zhao Z., Ding C., Pan L. *J. Opt.*, **19**, 025603 (2017).
19. Guo L., Chen Y., Liu X., Liu L., Cai Y. *Opt. Express*, **24**, 13714 (2016).
20. Zhang Y., Wang H., Ding C., Pan L. *Phys. Lett. A*, **381**, 2550 (2017).
21. Odintsov V.I., Sokolova E.Yu. *Quantum Electron.*, **24**, 723 (1994) [*Kvantovaya Elektron.*, **21**, 778 (1994)].
22. Odintsov V.I., Sokolova E.Yu. *Opt. Spektrosk.*, **101**, 478 (2006).
23. Baranova N.B., Zel'dovich B.Ya. *Zh. Eksp. Teor. Fiz.*, **80**, 1789 (1981).
24. Akhmanov S.A., Dyakov Yu.E., Chirkin A.S. *Introduction to Statistical Radiophysics and Optics* (Berlin: Springer, 1988; Moscow: Nauka, 1981).
25. Baranova N.B., Zel'dovich B.Ya., et al. *Zh. Eksp. Teor. Fiz.*, **83**, 1702 (1982).